International Journal of Hydrogen Energy 174 (2025) 151219

Contents lists available at ScienceDirect

International Journal of Hydrogen Energy

journal homepage: www.elsevier.com/locate/he

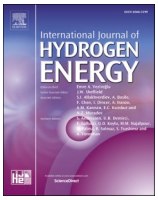

Poly(pentafluorstyrene) based ionomers for electrochemical hydrogen pumps I – How electrode properties affect the performance

M. Braig [a,b], H. Cho [c], C. Marchfelder [a,b], V. Atanasov [c], R. Zeis [a,b,d,*]

[a] Friedrich-Alexander-Universität Erlangen-Nürnberg, Faculty of Engineering, Department of Electrical Engineering, Cauerstraße 9, 91058 Erlangen, Germany
[b] Karlsruhe Institute of Technology, Helmholtz Institute Ulm, Helmholtzstraße 11, 89081 Ulm, Germany
[c] University of Stuttgart, Institute of Chemical Process Engineering, Böblinger Straße 78, 70199 Stuttgart, Germany
[d] University of Toronto, Faculty of Applied Science and Engineering, Department of Mechanical and Industrial Engineering, 5 King's College Road, Toronto, Ontario M5S 3G8, Canada

ARTICLE INFO

Keywords:
Electrochemical hydrogen pumping
Polybenzimidazole (PBI)
PWN70
Ionomer
Microstructure
Hydrophobicity

ABSTRACT

Electrochemical hydrogen pumps (EHPs) are a promising technology for isolating H_2 from gas mixtures. This work implements novel proton-conducting binders into gas diffusion electrodes (GDEs) and investigates full-cell EHPs with a phosphoric acid-doped polybenzimidazole membrane. The morphological GDE properties are investigated by scanning electron microscopy (SEM), energy-dispersive X-ray spectroscopy (EDX), and argon gas sorption, revealing an extremely high catalyst layer porosity with phosphonated poly(pentafluorstyrene) (PWN70) ionomer. Adding the nonionic surfactant Triton X-100 to the catalyst ink significantly improves the distribution of poly(pentafluorstyrene)-imidazole (PPFSt-Imi) binder, increasing electrode porosity and cell performance. Furthermore, the hydrophobicity of all catalyst layers is probed by dynamic vapor sorption. At 200 °C, the EHPs demonstrate 99.98 % H_2 purity and 100 % H_2 recovery from a reformate gas mix at 95 % power efficiency. A durability test at 1.6 A cm^{-2} proves stable electrode operation, highlighting the suitability of the employed binders for EHPs.

1. Introduction

Electrochemical hydrogen pumps (EHPs) based on polybenzimidazole (PBI) membranes doped with phosphoric acid (PA) offer a promising concept of separating H_2 from gas mixtures. Among the various polymer electrolyte membrane (PEM) based systems, the PBI membrane offers a high proton conductivity and exceptional thermal and chemical stability, making it an ideal candidate for EHP applications. High-purity H_2 can be recovered and simultaneously compressed with low energy consumption [1–3]. The operating temperature between 160 °C and 200 °C increases the robustness to platinum catalyst poisoning by CO or H_2S. These impurities are typically found in H_2-containing gas mixes derived from natural gas or biogas, like syngas and steam reformate [4]. In contrast, EHPs containing perfluorosulfonic acid (PFSA) membranes and ionomers exhibit optimum performance below 100 °C, which reduces the energy needed to heat up the EHPs. However, at this temperature their efficiency decreases severely if CO or CO_2 present in the gas feed at technically relevant conditions [5–7]. Poison mitigation strategies like periodic pulsing, O_2 bleeding (adding small percentages of O_2 or O_3 into the anode gas feed), or a regular change to pure hydrogen gas feed aim to reduce the contaminant's impact [5,8]. Yet, these complicate the operation and potentially damage the cells, e.g. voltage spikes might degrade the catalyst and O_3 impacts the membrane. Furthermore, liquid water present in the CL could inhibit the mass transport, which requires a sophisticated water management. Sulfonated poly(ether ether ketone) (SPEEK) membranes exhibit similar performance and limitations, as their operation temperature is also limited to 100 °C [9].

EHPs offer high operation flexibility since changing the external load's current can significantly adjust the H_2 transport across the membrane. The system is highly selective as only protons are conducted through the membrane, while impurities (e.g., CO, CO_2, H_2S, N_2) diffuse slowly through the PBI. Subsequently, a high H_2 recovery, high purity, and simultaneous high electrical efficiency can be achieved [10–12]. Furthermore, EHPs produce a continuous H_2 flow without pressure fluctuations, in contrast to the purified H_2 generated by the established

* Corresponding author. Friedrich-Alexander-Universität Erlangen-Nürnberg, Faculty of Engineering, Department of Electrical Engineering, Cauerstraße 9, 91058 Erlangen, Germany.
E-mail address: roswitha.zeis@fau.de (R. Zeis).

https://doi.org/10.1016/j.ijhydene.2025.151219
Received 1 October 2024; Received in revised form 17 July 2025; Accepted 25 August 2025
Available online 11 September 2025

pressure swing adsorption (PSA), which exhibits fluctuating flow rates due to the cyclic nature of the process [13]. While PSA may have an advantage regarding initial setup costs and industry maturity, EHPs have the potential for more straightforward operation and maintenance due to no moving parts or adsorbent replacements. Both palladium membrane separation and EHPs achieve high-purity hydrogen [14]. However, EHPs offer the advantage of using more cost-effective materials, reducing overall system costs. In addition, EHPs enable the on-site extraction of H_2 from the natural gas network, for example, at refueling stations for fuel cell vehicles, thereby avoiding the need for complex infrastructure or a separate network for hydrogen distribution.

Non-conducting fluorinated polymers like polytetrafluoroethylene (PTFE) are commonly employed as electrode binders with a PBI membrane [10,11,15–17]. These hydrophobic binders keep the PA electrolyte in the membrane and regulate the PA content and distribution in the electrodes. This is due to the liquid-repellent effect of PTFE, which prevents PA from leaking out of the cell. A high-performing catalyst layer (CL) must conduct protons and electrons, allowing for efficient reactant transport to the catalytic sites. A high PA content causes mass transport (MT) losses since the reactant diffusion is slower in PA than in the gas phase. On the other hand, a certain amount of PA in the electrode is necessary for good proton conductivity and a large triple phase boundary (TPB), which represents the electrochemically active surface area (ECSA). Therefore, a balanced PA distribution is vital to achieve good proton conductivity and MT simultaneously [18]. However, due to its isolating properties, PTFE does not contribute to the electrode conductivity. Furthermore, PTFE also decreases the TPB by blocking platinum catalyst particles.

Therefore, proton-conducting binders must be developed to enhance the conductivity and TPB in electrodes, thereby overcoming these limitations. Proton-conducting groups in ionomers are always polar, making the materials hydrophilic. Therefore, the ionomers also need to contain hydrophobic groups to prevent the flooding of the CL, which is an issue in EHPs, just like in fuel cells. Thus, ionomers exhibiting a combination of proton conducting and hydrophobic groups are expected to achieve high proton conduction and good MT simultaneously [19–21]. Furthermore, proton-conducting ionomers enlarge the TPB by conducting protons through the polymer film to the catalytically active sites. The previously published material PWN70 possesses a hydrophobic poly(pentafluorstyrene) backbone, partially phosphonated [20,22]. While PWN70 intrinsically conducts protons, PA doping further enhances its conductivity [23]. PWN70 has already been successfully employed in the CL of an EHP in combination with an ion-pair membrane, which allows an operating temperature of up to 220 °C [12]. Since the membrane properties significantly affect the PA distribution in the electrodes, different binders exhibit significantly different performance depending on the membrane used. The combination of PWN70 as an electrode binder with a PBI membrane in an EHP is investigated for the first time in this study.

While PA-doped PBI is an excellent proton conductor, it is unsuitable as an electrode binder. Low CL porosity and high polymer swelling result in sluggish MT in the electrodes, which causes poor performance despite the high proton conductivity [24,25]. To overcome these drawbacks, poly(pentafluorstyrene)-imidazole (PFFSt-Imi) binders with an alkyl chain were synthesized in this study. While the pentafluorstyrene backbone provides chemical and thermal stability, the imidazole groups bind PA molecules via ion pair interaction. Excess PA forms agglomerates, and this free PA serves as main proton conductor [26]. The binder's hydrophobicity is regulated by the length of an alkyl chain bound to the imidazole ring. Thus, the excellent conductivity of imidazole/PA is embedded in a hydrophobic structure, providing high activity and good PA distribution.

Gas diffusion electrodes (GDEs) fabricated with PWN70, poly (pentafluorstyrene)-imidazole (PPFSt-Imi), and PTFE binder were implemented into single-cell EHPs. Thermogravimetric analysis (TGA) was used to investigate the thermal stability of all ionomers. Extensive ex-situ characterization by scanning electron microscopy (SEM) coupled with energy-dispersive X-ray spectroscopy (EDX), argon gas sorption, and dynamic vapor sorption (DVS) investigates the morphological and physical properties of the catalyst layers. Furthermore, the dimensions of the binder particles were examined in different catalyst ink compositions by dynamic light scattering (DLS). All important binder properties are evaluated and correlated to the electrochemical performance.

2. Experimental

2.1. Binder synthesis

The structures of the high-temperature ionomers implemented into the GDEs are displayed in Fig. 1b. PPFSt, PWN70 and imidazole functionalized PPFSt (PPFSt-Imi) were synthesized according to the literature [22,27]. To obtain PPFSt-Imi-C6, PPFSt-Imi (1 g, 4.13 mmol) was dissolved in 40 ml N-methyl-2-pyrrolidone (NMP) at 90 °C for 3 h under argon protection in a round bottom flask equipped with a reflux condenser. After the complete dissolution of PPFSt-Imi, the polymer solution was cooled to room temperature (RT). An excess of iodohexane (2.68 g, 12.39 mmol) was added to the polymer solution at RT. The reaction mixture was stirred at 90 °C for 20 h, and the resulting product was isolated by precipitation in deionized water (DW). The polymer was thoroughly rinsed with DW several times and then dried in a vacuum oven at 60 °C for 24 h. Yield: 1.30 g (69 %). The PPFSt-Imi-C10 was synthesized using the same procedure as for PPFSt-Imi-C6. In this case, PPFSt-Imi (1 g, 4.13 mmol) and NMP (40 ml) were reacted with iododecane (3.39 g, 12.39 mmol). Yield: 1.41 g (67 %). PWN70 was synthesized as described in the literature [20,28].

2.2. Thermogravimetric analysis

The thermal stability of polymers was investigated by thermogravimetric analysis (TGA). The measurements were performed using a NETZSCH STA 499C test station. Samples were heated from 30 to 700 °C with a heating rate of 20 K min^{-1} under a gas mixture of 70 % oxygen and 30 % nitrogen by volume.

2.3. Nuclear magnetic resonance spectroscopy

The proton and fluorine nuclear magnetic resonance (^1H,^{19}F NMR) spectra were recorded at RT using a Bruker Avance 400 spectrometer (400 MHz for ^1H and 376 MHz for ^{19}F) in deuterated dimethylsulfoxide DMSO-d_6. Chemical shifts of the ^1H NMR spectra were referenced as DMSO-d_6 at 2.50 ppm as a reference.

2.4. Dynamic light scattering

Dynamic light scattering (DLS) with a Mastersizer3000 (Malvern Panalytical) was employed to select appropriate solvents for the catalyst ink of the ionomers. "Inks" were prepared with the same binder concentration as the catalyst inks used for electrode fabrication but without the Pt/C catalyst. Adding the Pt/C into the ink would increase the concentration of all solid contents to ~3 wt% in the dispersion. The high concentration causes multiple scattering effects, reducing the data quality. Furthermore, diluting the ink also affects the results, leading to unreliable size distributions [29]. Therefore, only the binder particle size was examined at comparable conditions. The samples were prepared as described in the Membrane Electrode Assembly Fabrication section, except that no Pt/C catalyst was added, and the tip sonication was omitted. The ink was stirred in the sample cell with a magnetic stirrer during the DLS measurement. 30 measurements were recorded and averaged for each ionomer.

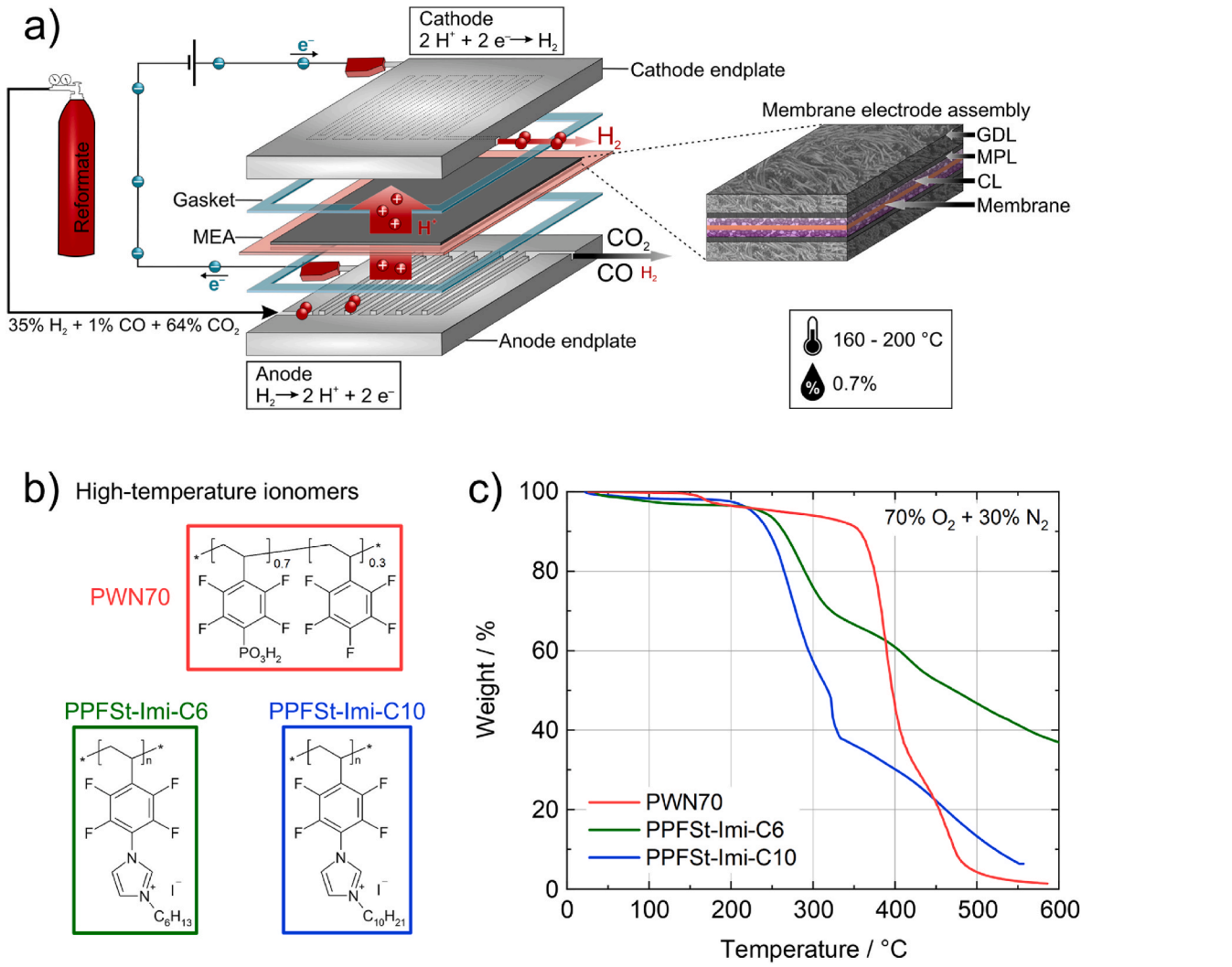

Fig. 1. a) EHP cell setup made of two stainless steel endplates with serpentine flow fields, the MEA consisting of the GDL with MPL, a spray-coated Pt/C catalyst layer (CL), and the PBI membrane. Hydrogen was isolated from a reformate containing 35 % H_2 + 1 % CO + 64 % CO_2 between 160 °C and 200 °C at 0.7 % RH. b) Structures of the investigated high-temperature ionomers. c) TGA of the ionomers in 70 % O_2 + 30 % N_2 atmosphere.

2.5. Scanning electron microscopy and energy-dispersive X-ray spectroscopy

SEM images of the CL surface and the gas diffusion layer (GDL) were recorded with an LEO 1550 VP (Carl Zeiss) instrument and an in-lens detector at 3 kV acceleration voltage. For EDX mapping, the voltage was raised to 10 kV to increase the signal.

2.6. Gas sorption

Argon sorption isotherms were recorded with an autosorb iQ (3P Instruments). An external cryotune temperature controller (3P Instruments) controlled the temperature to 87 K, corresponding to the boiling temperature of Argon. The Brunauer-Emmett-Teller (BET) surface area was calculated using the Quantachrome ASiQwinTM software from the obtained isotherms. The R^2 of the BET fit was over 0.999 in all cases. Furthermore, the pore size distributions were determined by quench solid density functional theory (QSDFT) calculations assuming slit pores in the same software. Due to the dimensions of the sample holder, the GDL and the GDEs had to be sliced into small fragments. Before each measurement, the sample was outgassed at 150 °C under vacuum for 20 h to remove adsorbates from the sample surface.

Argon sorption was performed on the as-received GDL and the fabricated GDEs. The measured GDEs were identical to those employed in the EHPs. Since the weight of the GDL and the CL were measured during the coating process, the sorption of the GDL can only be subtracted from the GDE sorption to obtain the morphology of the CL. All presented sorption measurements of the electrodes describe only the CL, not the entire GDE.

2.7. Dynamic vapor sorption

The hydrophobicity of all GDEs was investigated by dynamic vapor sorption (DVS) in a Q5000SA sorption analyzer (TA Instruments). The prepared GDEs were cut into small pieces and dried at 80 °C for 6 h. After transferring the samples into the instrument, the remaining residues were removed in an isothermal step at 60 °C for 5 h under a dry N_2 gas flow. The adsorption and desorption isotherms were recorded at 25 °C up to 90 % relative humidity (RH). Data was recorded in increments of 1 % RH up to 5 %. Beyond 5 % RH, the interval was increased to 5 %. Each RH was maintained for 90 min to ensure equilibrium conditions, with the exceptions being 80 % and 85 %, where the duration was extended to 120 min, and at 90 %, where the duration was extended to 180 min. The desorption isotherms were recorded at identical RHs and dwell times, except no points were recorded between 0 and 5 % RH. Analogous to the argon sorption measurements, the sorption of

only the CL was calculated by subtracting the sorption on the GDL from the sorption on the complete GDE. All DVS measurements represent the sorption on the CL only.

2.8. Gas chromatography

Gas samples were taken at the cathode outlet using a gas-tight container with a manual valve at its inlet and outlet. After reaching a stable EHP operating point, the sample container was flushed for 30 min with the cathode gas. To take a sample, the valve at the cylinder outlet was closed. Subsequently, the container was pressurized to 200 mbar since a slight overpressure was needed to flow the gas from the container into the gas chromatograph (GC). When the desired pressure was reached, the inlet valve was also closed. Afterward, the cylinder was connected to the GC with a gas-tight Swagelok tube to prevent contamination by ambient gas. A Shimadazu GC-2030 N with two barrier discharge detectors was employed to measure contaminants in the purified hydrogen. Due to the detection limit of <0.1 ppm for CO and CO_2, accurate quantification is guaranteed even in the low ppm range.

2.9. Membrane Electrode Assembly Fabrication

All membrane electrode assemblies (MEAs) were fabricated with commercial PBI membranes (Dapozol M40, Danish Power Systems, 40 μm thickness undoped) and in-house fabricated GDEs. The membranes were doped in 85 % PA (AnalaR Normapur, VWR Chemicals) at room temperature for at least 1 month. Before cell assembly, the membranes were wiped on a paper cloth to achieve a doping level of 9 g PA per 1 g PBI.

Catalyst inks containing a 20 wt% Pt on carbon black catalyst (Alfa Aesar) and different binders were spray-coated onto a commercial GDL with a microporous layer (MPL). The H14CX653 GDL (Freudenberg) was employed unless indicated otherwise. The non-ionic surfactant Triton X-100 was added to the ink to improve its homogeneity, where indicated.

The ink with the PTFE binder was prepared using a 1:1 ratio of isopropanol (IPA) and water, a standard composition for catalyst inks with PTFE binders [18,30,31]. The other examined binders were first dispersed in dimethylacetamide (DMAC, 99 %, thermo scientific) at a concentration of 5 wt% by stirring. Subsequently, this dispersion was added to a 3:1 mixture of IPA:water (and Triton X-100 where applicable) and stirred for 1 h. The wt% of Triton X-100 in the ink was identical to the binder percentage. Afterward, the Pt/C catalyst was added, and the ink was finally homogenized with a tip sonicator for at least 30 s. The content of all solids in the ink was 3.3 wt%, with 3.0 wt% being the Pt/C catalyst and 0.3 wt% the respective binders.

The prepared ink was then sprayed onto the MPL of the GDL with an airbrush system with N_2 at ~2 barg. The GDL was placed on a heating plate with ~90 °C to evaporate the solvents during spray coating. After every layer, the ink was placed in an ultrasonic bath to ensure the ink remained homogeneous. The ultrasonic bath was heated to 40 °C for the ink prepared with Triton X-100, which decreased the ink's viscosity. At ambient temperature, the Triton X-100 ink could not be sprayed. The catalyst loading was 1.0 mg Pt cm-2 for all prepared GDEs. The binder content in the dry CL was 11 wt% for PTFE (prepared with a 60 % PTFE dispersion in water, Sigma-Aldrich) and 10 wt% for all other binders, corresponding to an ionomer/carbon ratio of 0.15 and 0.14, respectively.

The EHP setup is displayed in Fig. 1a. Single cells were assembled with identical GDEs on the anode and cathode. PTFE gaskets (120 μm) were used to determine the compression, and a PEEK sub-gasket (25 μm) was placed between each GDE and the membrane, setting the active area to 4 cm^2. Stainless steel endplates with serpentine flow fields served as current collectors. 8 screws in the endplates were tightened with 2 Nm to achieve good conductivity between all cell components and to ensure gas tightness.

2.10. Electrochemical characterization

All cells were heated to 160 °C under dry H_2 gas feed on the anode in a custom-built test station. The cell temperature was measured by a thermocouple inserted into the center of each endplate and controlled by heating pads on the outer side of each endplate. Mass flow controllers regulated the gas flows. The gas feed humidification was adjusted to reach 0.7 % RH at each cell temperature. The dew points were 30 °C, 39 °C, and 47 °C at a cell temperature of 160 °C, 180 °C, and 200 °C, respectively. In pre-tests a higher RH of only 1.6 % caused MEA flooding, especially at high currents, due to the hygroscopic nature of PA. The gases were preheated by heating coils before being supplied to the EHP. No gas flow was applied on the cathode, and all EHPs were operated without back pressure.

The cells were conditioned for 48 h at 0.2 A cm^2 at 160 °C with pure H_2 at the stoichiometry $\lambda_{H2} = 1.8$. Afterward, the performance was characterized using electrochemical impedance spectroscopy (EIS) and potential curves (PCs) with pure H_2 or 35 % H_2 + 1 % CO + 64 % CO_2 gas feed at different temperatures and stoichiometries. After adjusting the temperature, the EHP was operated for at least 12 h before the respective characterization to achieve stable operation. The EIS was recorded from 200 kHz to 100 mHz with an amplitude of 0.025 A cm^{-2}. More details on the EIS measurements can be found in part II [32]. The membrane and total cell resistances were determined at the high-frequency and low-frequency intercepts in the Nyquist plot, respectively. The difference between the total and membrane resistance represents the electrode resistance.

The hydrogen recovery rate and the consumed power determine the efficiency of an EHP. The recovered hydrogen (see equation (1)) represents the share of evolved hydrogen at the cathode ($F_{H2,out}$) compared to the hydrogen gas supplied to the anode ($F_{H2,in}$). If a part of the hydrogen feed cannot be isolated to the cathode, it is considered lost. Literature data showed a faradic flow, demonstrating an excellent agreement between the measured hydrogen flow at the cathode and the theoretical value [10,16,33]. Therefore, the hydrogen recovery corresponds to the inverse of the stoichiometry λ with excellent accuracy.

$$\text{Hydrogen recovery} = \frac{F_{H_{2,out}}}{F_{H_{2,in}}} = \frac{1}{\lambda} \quad (1)$$

The power efficiency (see equation (2)) can be calculated with the heat of combustion of hydrogen ($\Delta H_{combustion}$, 142 MJ kg^{-1}) [10]. The applied power ($P_{applied}$) is the product of the supplied current and the cell voltage.

$$\text{Power efficiency} = \frac{F_{H_{2,out}}\,\Delta H_{combustion} - P_{applied}}{F_{H_{2,in}}\,\Delta H_{combustion}} \quad (2)$$

3. Results and discussion

Imidazolium functionalized PPFSt has been previously synthesized and reported [27]. In this study, a methyl group was introduced onto an imidazole-functionalized PPFSt to convert the imidazole to a methylimidazolium (Me-PPFSt-Imi). However, when PPFSt was 100 % imidazole-functionalized, after methylation (Me-PPFSt-Imi), the product became water-soluble due to its high ion-exchange capacity. Therefore, in the current study, long hydrophobic alkyl chains were introduced by using either iodohexane (I-C6) or iododecane (I-C10) via nucleophilic substitution in the imidazole group. As can be seen in Figure S. 3 in the ^1H NMR spectra of the PPFSt-Imi-C6 and -C10, a new peak appeared at 4.37 ppm assigned for (Imi)N-C$\underline{H}_2$-R(H_c protons), indicating a successful quaternization of the imidazole ring by C6 and C10 alkyl chains. The Ion exchange capacity (IEC) was determined to 2.40 mmol g^{-1} for PWN70, 2.20 mmol g^{-1} for PPFSt-Imi-C6, and 1.96 mmol g^{-1} for PPFSt-Imi-C10.

Since EHPs based on a PA-doped PBI membrane are typically operated at elevated temperatures above 160 °C, the ionomers must exhibit

high thermal oxidative stability. TGA results presented in Fig. 1c indicate small weight loss for all binders below 200 °C, which can be assigned to the evaporation of water adsorbed to the polar groups of the polymers [27]. Between 200 and 350 °C anhydride formation of the phosphonated groups in PWN70 releases water, reducing the sample mass. The decomposition of the PWN70 polymer backbone begins only around 350 °C, making it a suitable candidate for electrode ionomers in EHPs [20,22,28]. Both PPFSt-Imi-based ionomers exhibit substantial weight loss starting around 215 °C. The investigation by TGA, coupled with Fourier-transform infrared spectroscopy (FTIR) of a Me-PPFSt-Imi polymer in the literature, showed a similar thermal decomposition behavior to that of the examined binders in this study [27]. Since this material is identical in structure except for the length of the alkyl chain, the results are likely transferable. CO and CO_2 were detected only above 255 °C, indicating degradation of the polymer backbone. However, the methyl group was split off as iodomethane through nucleophilic substitution by the iodide already at 215 °C. Since the ionomers of this study also exhibit pronounced weight loss at the same temperature, their longer alkyl chain (C6 or C10) decomposes at a similar temperature. However, substituting I^- - with H_2PO_4- as a counter ion stabilized the PPFSt-Imi significantly, increasing the decomposition temperature to 320 °C [27]. PA migrating from the PBI membrane into electrodes during the break-in of the EHP substitutes the iodide with $H_2PO_4^-$, stabilizing the polymer. Therefore, PA-doped PPFSt-Imi tolerates the selected operating temperature range between 160 and 200 °C. This migration is promoted by the high PA doping level of the PBI membrane in this study, which is 9 g PA per 1 g PBI, allowing for a substantial amount of PA leaching.

3.1. Ink composition

Due to different binder-solvent interactions, the ink composition of each binder must be optimized. Since the employed binders in this study contain polar (phosphonic acid and quaternary ammonium) and nonpolar (fluorinated and alkylated) functional groups, a mixture of solvents with different polarities typically produces suitable binder distributions [34]. The interactions of the binder, the catalyst, and the solvent determine the microstructure of the CL. A well-distributed binder provides a large TPB and high porosity, essential for proton transport (PT), charge transfer, and mass transport in the electrodes.

The severe impact of the solvents and the binder particle sizes on the performance of a fuel cell has been demonstrated for PWN70 [35] and Nafion [36,37]. An intermediate binder particle size similar to the size of the Pt/C particles was identified as optimal [37]. Small particles form a continuous film, benefiting the PT in the CL. However, fine particles with a similar size to the pores of the Pt/C catalyst (<20 nm) block the pore network, hindering the gas transport. Conversely, large binder particles form an isolated ionomer film with minimal contact to the Pt/C catalyst. While the unfilled catalyst pores provide excellent mass transport, Pt's insufficient contact with the ionomer results in a reduced TPB. Thus, the electrocatalytic activity and proton transfer are poor. Therefore, an intermediate particle size benefits cell performance, balancing PT, TPB, and MT. A uniform binder size is desirable since it produces homogeneous CLs without larger agglomerations. Lastly, a well-dispersed binder is essential for producing mechanically stable GDEs and controlling the PA distribution in the CL.

The particle sizes of the employed ionomers in different IPA:water ratios are presented in Fig. 2. A reliable determination of the PTFE particles was not possible due to the milky dispersion, which resulted in a poor signal-to-noise ratio. While dilution of the sample could potentially improve data quality, it also affects particle size [29]. Therefore, the measured values would differ from the utilized catalyst ink. Furthermore, the diameter determined by DLS is typically overestimated since a few large particles dominate the signal [38]. Thus, the DLS data only yields qualitative information.

All measured dispersions have the same binder concentration (0.3 wt %) as the inks used for coating the CLs. Preliminary CL coating tests with the PPFSt-Imi binders showed insufficient mechanical electrode stability if the ink was composed of only IPA and water, as the CL flaked off the MPL. To improve the electrode stability, DMAC was added to the ink. Furthermore, a better fuel cell performance has been reported with a PWN70 binder for an ink containing DMAC compared to only IPA and water [35]. Therefore, all ionomers were pre-dispersed in DMAC at a concentration of 5 wt%. Subsequently, this dispersion was added to the respective IPA: water mixtures (and Triton X-100 surfactant, where applicable). Adding DMAC to the solvent mixture slows down its evaporation due to the high boiling temperature of DMAC. Thus, DMAC also reduces crack formation, which can be caused by fast solvent evaporation [39,40]. Furthermore, DMAC significantly impacts the binder distribution, since it evaporates after the other solvent components. Therefore, the binder is mainly in contact with DMAC before solidifying.

For all investigated binders, the particle size decreases at higher IPA content. While the polar binder groups interact with polar solvents, the

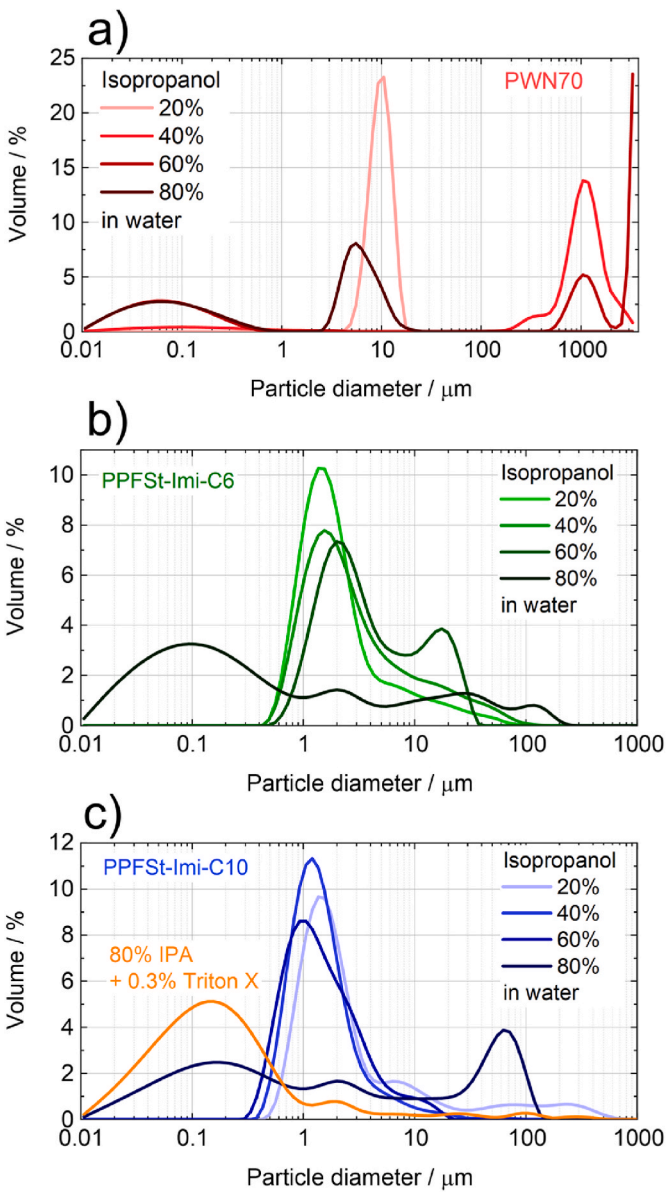

Fig. 2. Volumetric particle size distribution of a) PWN70, b) PPFSt-Imi-C6, and c) PPFSt-Imi-C10 in different IPA/water mixtures. The ionomers were dissolved in DMAC before adding IPA/water, so every sample also contains 6.5 % DMAC.

hydrophobic backbone of the polymer particles repels them. Instead, the hydrophobic backbone interacts with other particles' backbone, forming agglomerations. Increasing the IPA content and, thereby, reducing the polarity of the solvent mixture increases the interaction of the backbone with the solvent. This causes agglomerations to break up, forming smaller particles in the ink. These finer particles improve the distribution of the binder in the dry electrode, enhancing EHP performance. Therefore, all inks for the spray-coating of the CLs were prepared with a high IPA content (IPA: water 3:1). Two distinct particle sizes, between 0.01 and 1 μm and 2 and 20 μm, are present in the PWN70 dispersion. A broader particle size distribution (PSD) is measured in the dispersion with both PPFSt-Imi binders, although the longer alkyl chain produces larger agglomerations due to its increased hydrophobicity. By adding Triton X-100 surfactant to the PPFSt-Imi-C10 binder, the particle size was reduced, and a relatively narrow PSD, mainly between 0.01 and 3 μm, was obtained. Triton X-100 also demonstrated a similar effect for a dispersion containing Nafion ionomer, reducing the particle size [41]. The hydrophobic groups of the surfactant and the ionomer interact in the dispersion, forming micelles and preventing the entanglement of the ionomer chains. Thus, Triton X-100 supports the dispersion of the polymer by reducing the agglomerate size, resulting in a more homogeneous distribution within the dried catalyst layer. This improved dispersion can lead to more accessible catalytic sites and enhanced mass transport properties within the electrode, improving the EHP performance. The PWN70 and the PPFSt-Imi-C10 + Triton X-100 inks exhibit suitable PSDs for coating electrodes.

3.2. Electrode morphology

SEM images of the CL surface of all prepared GDEs are presented in Fig. 3. The application of PTFE and PWN70 as binders results in homogeneous electrodes. While the PTFE CL exhibits a certain roughness, the PWN70 electrode is "flat" (see also SEM images at lower magnification in the supporting information, Figure S. 1). Contrarily, both PPFSt-Imi binders produce a very uneven electrode surface due to the broad PSD in the respective inks. The chain length of C10 resulted in larger particles dispersed in the ink than in the case of C6, leading to an even less homogenous surface, confirming the interpretation of the DLS data from Fig. 2. Furthermore, Triton X-100 significantly improves the homogeneity of the electrode caused by the narrow PSD in the ink. However, the electrode is still not as smooth as when PTFE or PWN70 is employed as binder, indicating relatively poor film formation properties for the PPFSt-Imi binders.

The employed H14CX653 GDL is coated with a crack-free MPL with a high polymer content (see Fig. 3f). While the very hydrophobic MPL prevents acid leaching from the MEA into the carbon fiber substrate of the GDL, its relatively low porosity poses a barrier to mass transport for the supplied gas [42]. Therefore, this GDL leads to a high proton

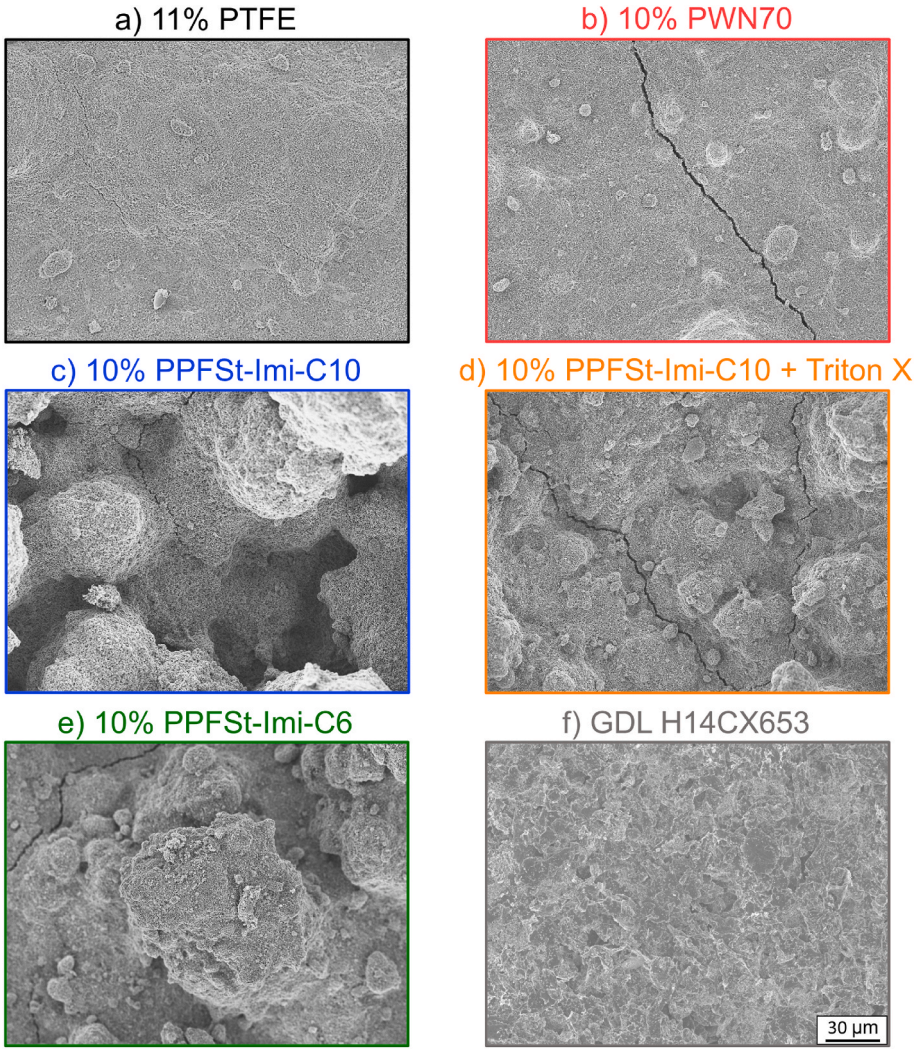

Fig. 3. SEM images of the catalyst layer surface of the spray-coated GDEs with a) 11 % PTFE, b) 10 % PWN70, c) 10 % PPFSt-Imi-C10, d) 10 % PPFSt-Imi-C10 and Triton X-100, and e) 10 % PPFSt-Imi-C6. f) the MPL of the employed Freudenberg GDL H14CX653.

conductivity in the MEA but impedes the diffusion.

The distribution of each component in the CL, as mapped by EDX, is shown in Fig. 4. The fluorine signal represents the binders. Several polymer accumulations, up to 10 μm in diameter, are present in the PTFE CL. PTFE interacts strongly with itself rather than with ink solvents, as PTFE has no polar groups and is highly hydrophobic. Therefore, certain agglomerations are always present when PTFE is employed as binder [43–45]. The carbon and fluorine signals match well for the other binders, suggesting that all ionomers are well distributed. The poor film formation properties of the PPFSt-Imi binders also cause an uneven electrode structure, despite the binders being relatively well distributed. Areas without any signal can be observed in all electrodes due to the roughness of the CL surface. The uneven surface casts "shadows", preventing the signal originating in these areas from reaching the detector. These dead areas are represented by a weak signal for all probed elements and do not indicate areas without ionomer. No significant interactions between the binder and the Pt catalyst particles were found. The binders are not particularly concentrated around the few Pt agglomerations, but they are also located on top of the Pt particles. Interaction of ionomer binders with the Pt surface has been well described for phenyl and ammonium containing binders [46]. The adsorption of phenyl moieties has appeared to be substantial and may cause a drop in performance due to contamination of the Pt surface by the phenyl ring. Therefore, in order to suppress the poisoning of the catalyst by the binder, we selected ionomers having bulky anion exchange functional groups and perfluorinated phenyl rings (see the structures in Fig. 1b).

The morphology of the fabricated GDEs was also investigated by argon sorption. Fig. 5 presents all CLs' surface area (SA) and pore volume, and the employed GDL H14CX653. Gas sorption of argon yields a

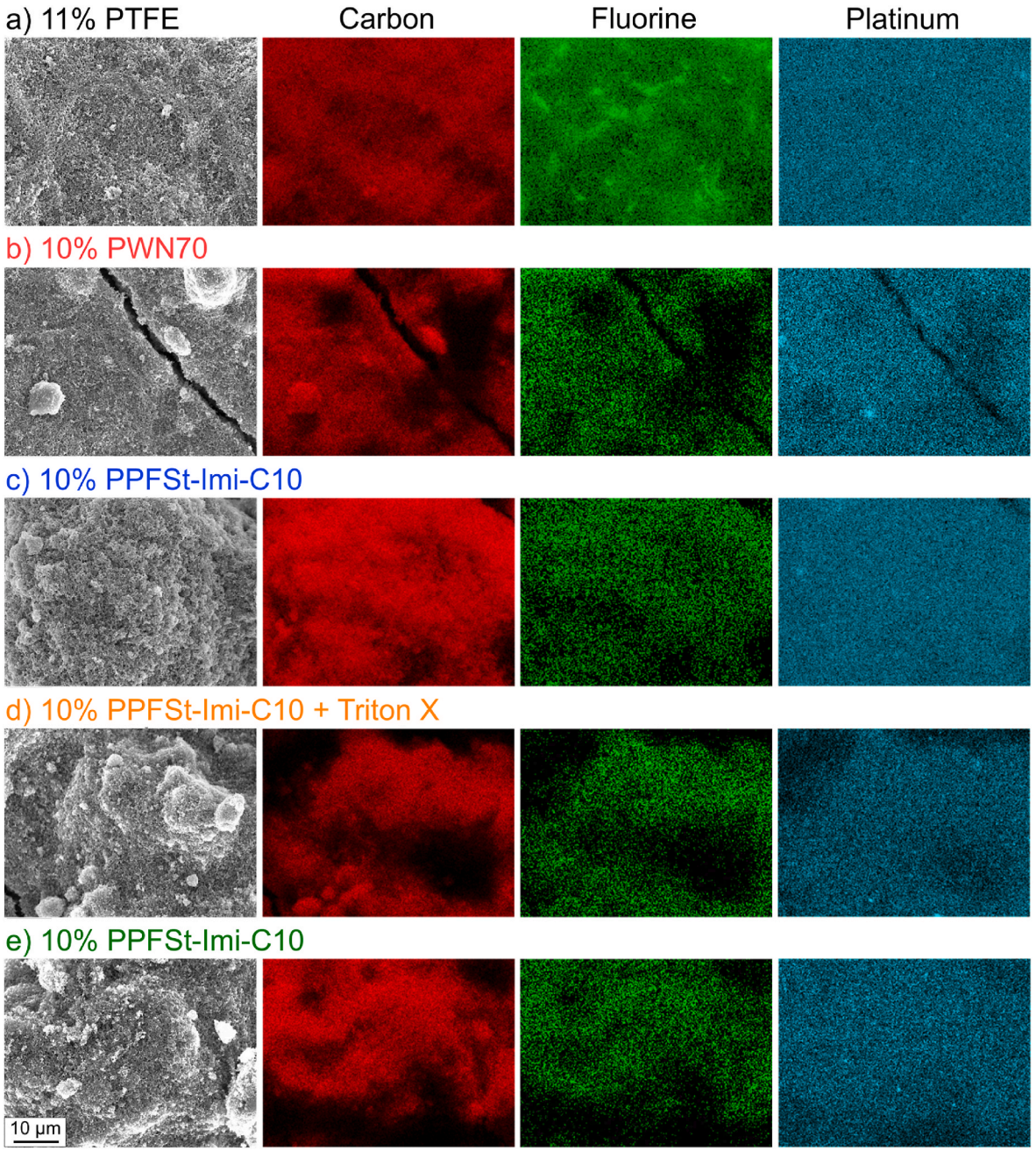

Fig. 4. SEM images and the corresponding distribution of carbon, fluorine, and platinum of the catalyst layers measured by EDX fabricated with a) 11 % PTFE, b) 10 % PWN70, c) 10 % PPFSt-Imi-C10, d) 10 % PPFSt-Imi-C10 + Triton X-100, and e) 10 % PPFSt-Imi-C6.

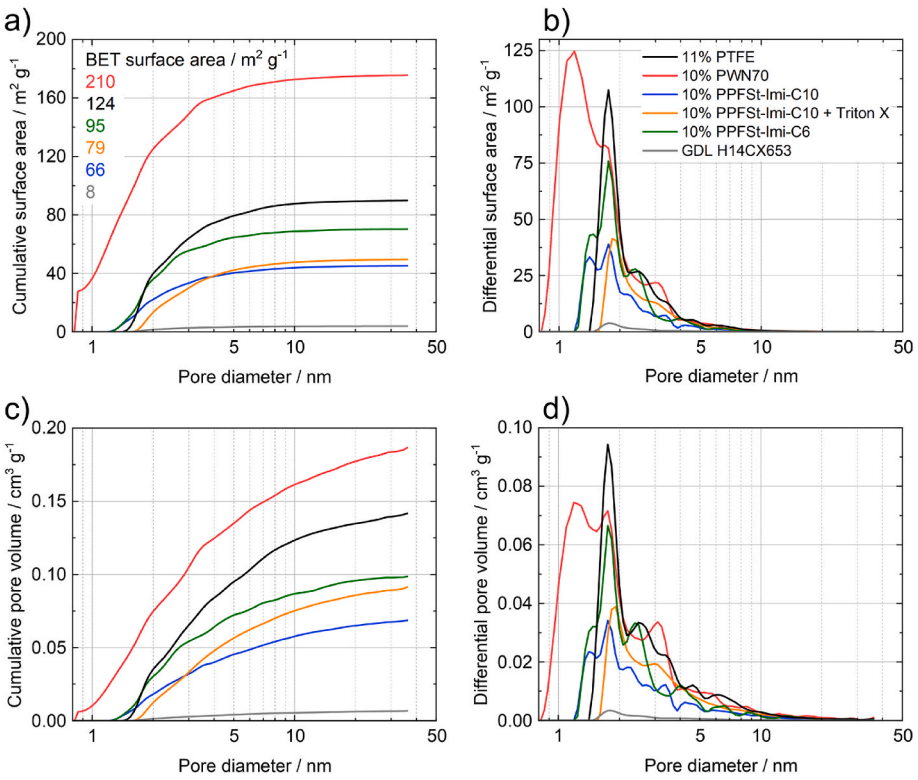

Fig. 5. a) Cumulative surface area, b) differential surface area, c) cumulative pore volume, and d) differential pore volume of the spray-coated catalyst layers and the employed GDL H14CX653. QSDFT calculations of Argon sorption isotherms were determined from the data. The BET surface area calculated from the same isotherms is indicated in a).

more accurate result than the often-employed nitrogen sorption. The nitrogen molecule exhibits a quadrupole moment, which leads to its interaction with specific surface groups. Nitrogen adsorbs onto the surface in different orientations, depending on these groups, which influences the determined morphology [47]. Argon is a single-atom gas and, therefore, has no quadrupole moment. Only the Van-der-Waals interactions determine the adsorption of Argon on the probed surface. Since the surface groups of the measured sample do not influence the measurement, argon sorption enables a more accurate identification of morphology.

The SAs of the CLs calculated by the BET and the QSDFT methods indicate identical orders regarding porosity, although the BET SA is higher for all cases. While the BET equation is widely used to determine the SA, surface adsorption often does not perfectly represent the model, which assumes the formation of an argon monolayer on the sample. Other factors, such as multilayer adsorption and interactions between adsorbate molecules, affect the accuracy of the BET analysis. QSDFT calculations are based on more sophisticated theoretical models, which better represent the multilayer adsorption and the pore filling at different partial pressures [48]. However, the accuracy of the QSDFT method strongly depends on assumptions about the interactions between adsorbate-adsorbents. In this case, the model for argon-carbon (slit pores) was applied, although the CL contains Pt and the respective binder as well. A fit error between 0.4 % and 3.5 % was determined for the CLs containing PWN70 and PPFSt-Imi-C10 + Triton X-100, respectively. BET and QSDFT exhibit different limitations, resulting in distinct SA results. However, the SAs determined by both methods are still in relatively good agreement. Furthermore, a pore size distribution is only obtained by the QSDFT model.

The CL fabricated with PWN70 as a binder exhibits the highest porosity. The very high BET SA of 210 $m^2\ g^{-1}$ even exceeds the pristine Pt/C catalyst powder, which was determined to 141 $m^2\ g^{-1}$. Thus, the binder must be well dispersed and not clog the micropores of the Pt/C. Furthermore, the binder itself is likely porous. Jung et al. have already demonstrated that PWN70 forms a porous film when cast with certain solvents [35]. Our results confirm the formation of pores in the PWN70 polymer with DMAC as solvent. Micropores in the binder are beneficial, as they improve gas diffusion in the CL and potentially reduce the adsorption of PA on the platinum surface [25]. The high SA of the CL may indicate a large TPB, although gas sorption provides no information about the actual ECSA. The CLs containing PTFE or the PPFSt-Imi binders are significantly less porous at a BET SA between 66 and 124 $m^2\ g^{-1}$. Compared to PWN70, this lower SA is mainly caused by less accessible pores <2 nm. Thus, these micropores are likely located in the PWN70 film itself. While the PPFSt-Imi binders might still allow the utilization of platinum particles in the binder-filled pores due to their proton conductivity, PTFE renders them inaccessible.

Adding Triton X-100 to the PPFSt-Imi-C10 binder shifts the pore size distribution towards larger diameters. The PSD in the inks presented in Fig. 2 already indicates a shift towards significantly smaller binder agglomerations when Triton X-100 is added, and these smaller ionomer particles are accommodated within smaller Pt/C pores. Since the binder is increasingly located in micropores, fewer binders are in mesopores. Thus, Triton X-100 increases the pore volume of the CL, which supports mass transport through the pore network. A longer alkyl chain on the PPFSt-Imi binders reduces the CL porosity due to larger particles in the ink (see Fig. 2).

The CL hydrophobicity determines the PA migration from the membrane into the CL, which is simultaneously essential for PT, TPB, and MT. Dynamic vapor sorption (DVS) was used to probe the hydrophobicity of all GDEs. Although water sorption at 25 °C does not perfectly represent the operating conditions in the EHP, where the CL interacts with PA between 160 and 200 °C, it does allow a qualitative assessment. While PTFE is the most hydrophobic material, the electrode morphology and the binder distribution also play a significant role [49]. In Fig. 6a, the water adsorption isotherms of all catalyst layers are

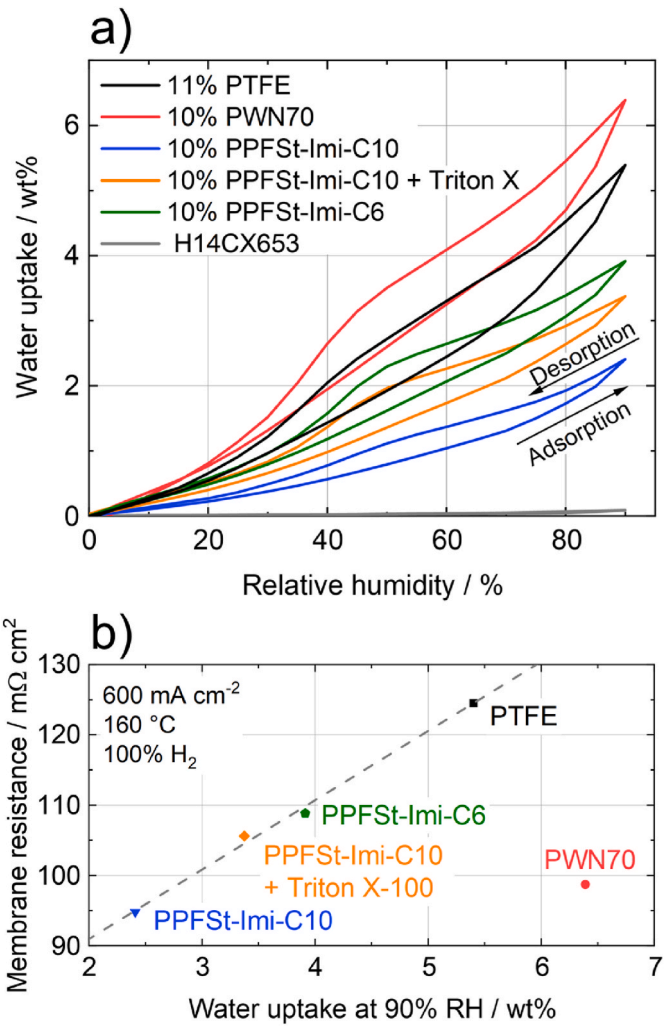

Fig. 6. a) Water vapor sorption isotherms of the catalyst layers and the GDL H14CX653 measured at 25 °C, and b) correlation of the membrane resistance and the GDE hydrophobicity represented by the water uptake at 90 % RH.

presented. The PWN70 CL adsorbs the most water due to its high content of polar groups. Surprisingly, the PTFE CL shows the second highest water uptake, while all CLs made with PPFSt-Imi binders exhibit a higher hydrophobicity. As shown in the binder distribution mapped by EDX in Fig. 4, PTFE forms the most agglomerations during the coating process. A large part of the binder inside these agglomerations is "dead material". It does not contribute to the hydrophobicity of the electrode since only the surface of the binder produces the hydrophobicity. On the contrary, the PPFSt-Imi binders are well distributed, increasing the binder SA in the CL. Thus, the binder distribution dominates the hydrophobic properties of the fabricated CLs over the intrinsic properties of the binder.

The longer alkyl chain of the PPFSt-Imi-C10 results in a significantly more hydrophobic CL, while the addition of Triton X-100 makes the electrode more hydrophilic. Since water vapor primarily adsorbs onto the polar groups of the ionomer, the higher adsorption indicates more exposed imidazole groups when the surfactant is employed. If the polar groups are not accessible to water vapor, they will likely not come into contact with PA either. Therefore, the surfactant should also increase the accessibility of imidazole groups to PA interaction, thereby improving the proton conductivity in the ionomer film. Subsequently, the EHP performs worse without Triton X-100, since the PPFSt-Imi binders only reach their full conductivity potential when doped with PA.

The water uptake of the CLs at 90 % RH and the membrane resistance of the corresponding EHPs show a linear correlation (see Fig. 6b). If a CL is more hydrophobic, less PA migrates from the membrane into the electrodes. Subsequently, more PA remains in the PBI matrix, increasing its conductivity. Only the PWN70 CL shows a significantly better conductivity than its hydrophobic properties suggest. While the high-water adsorption indicates a high PA content in the CL, the membrane resistance remains relatively low and similar to that of the most hydrophobic CL with the PPFSt-Imi-C10 binder. Low interfacial resistances between the membrane and the GDEs, due to the homogeneous and flat CL structure (see SEM image in Fig. 3), might improve conductivity in the cell. Furthermore, a homogenous electrode structure might improve its electrical conductivity since the carbon network is better connected [50].

3.3. Electrochemical characterization

Fig. 7 presents PCs with pure H_2 gas feed at 160 and 180 °C, along with the corresponding membrane and electrode resistances determined by EIS (EIS data are provided in the Supporting Information, Fig. S2). At 160 °C, the PWN70 MEA performs best, followed by the PTFE cell (see Fig. 7a). Both EHPs exhibit a similar electrode resistance, significantly lower than all PPFSt-Imi MEAs (see Fig. 7d). A reduced membrane resistance for PWN70 compared to the PTFE cell (see Fig. 7c) is the main reason for its lower power consumption.

Surprisingly, the electrode resistance of the PPFSt-Imi binders is lower for the longer alkyl chain. The higher water sorption, as determined by DVS, and the higher membrane resistance for the C6 chain suggest a higher PA in this electrode, which should improve proton conductivity but inhibit mass transport. Furthermore, the PPFSt-Imi-C6 binder showed higher porosity and surface area in the argon sorption results (see Fig. 5), which suggests a higher TPB leading to better kinetics and a facilitated MT. The fact that the PPFSt-Imi-C10 binder still performs better must be related to the intrinsic properties of the binder. Since each cell process strongly depends on the PA distribution, it is likely the cause of the better performance with the longer alkyl chain. The addition of Triton X-100 improves the electrode resistance, as the corresponding CL was shown to be significantly more homogeneous. Therefore, a better polymer film enhances the PT and the kinetics by enlarging the TPB. Since the pore volume of the CL also increases, the MT improves as well.

At 180 °C, the electrode resistances of the PTFE and PWN70 cells increase due to dehydration of the PA electrolyte at higher temperatures [51,52]. The formation of polyphosphates reduces the PT of the electrolyte and increases its viscosity, which worsens the electrolyte distribution in the carbon network [43]. However, the resistance increase is less pronounced for the PWN70 binder. A certain part of the PA electrolyte is immobilized on the ionomer due to its strong bond to the phosphonic acid group of PWN70 [20]. Dehydration of these bonded PA molecules is unlikely, and the PWN70-PA ensembles retain their conductivity at higher temperatures. However, the remaining free PA molecules form polyphosphates, reducing electrode performance analog to the cell utilizing PTFE binder. Contrarily, the electrode resistance decreases significantly at 180 °C for the PPFSt-Imi binders. While the electrode resistance of all PPFSt-Imi MEAs is still considerably higher compared to PWN70, the PPFSt-Imi-C10 cells exhibit a better EHP performance (see Fig. 7b) than PTFE due to the lower membrane resistance. The PPFSt-Imi binders are relatively inactive at 160 °C, but their proton conductivity increases significantly at 180 °C. The interaction of the PA with the binder is likely enhanced at a higher temperature, increasing its ionic conductivity. Furthermore, PA leaching from the PBI membrane into the electrodes increases at higher temperatures, improving the electrodes' proton transport [53]. Due to the higher interaction of PA with the PPFSt-Imi ion-pair binders, PA is retained in the electrodes. At 180 °C, a PPFSt-Imi-C1 membrane showed significantly higher conductivity retention than PBI over time, which indicates a stronger interaction between PA and the binder over the membrane

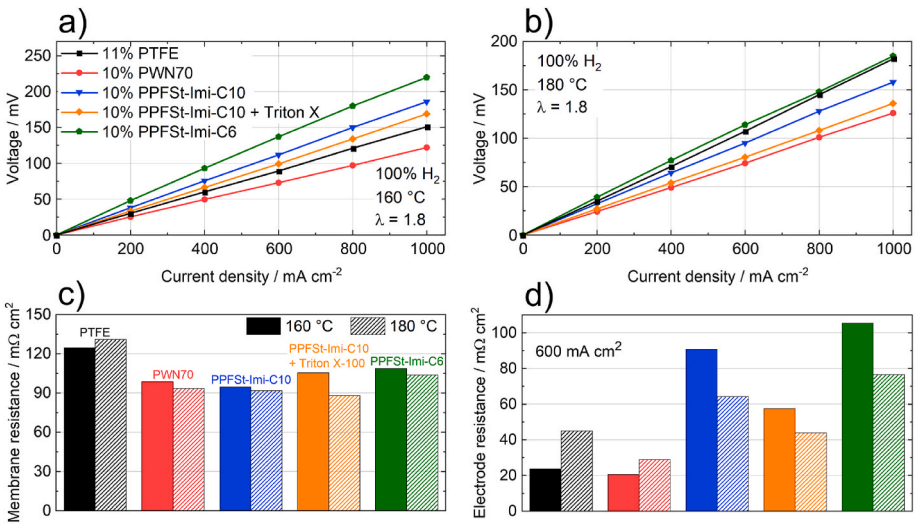

Fig. 7. EHP polarization curves with 100 % H_2 gas feed humidified to 0.7 % RH at a) 160 °C and b) 180 °C, and the resistances of c) the membrane and d) the electrodes determined by EIS at 0.6 A cm^{-2}.

[27].

The argon sorption showed a certain filling of tiny Pt/C pores with the PPFSt-Imi binders. The catalyst in these pores appears to be mostly inactive at 160 °C due to the binder's low conductivity, which contributes to the high electrode resistance. As the temperature increases to 180 °C, the TPB increases as protons are transported effectively through the binder film into the catalyst and micropores. PWN70 and PPFSt-Imi-C10 exhibit better performances at higher temperatures than PTFE due to the conductivity improvement of the PA/ionomer groups. At the same time, the dehydration of free acid in the PTFE CL reduces the conductivity.

Currently, H_2 is produced by steam reforming natural gas, which results in a mixture of H_2, CO_2, and CO [4]. To simulate the performance of the EHP under a typical gas mix, the cell was fed with 35 % H_2 diluted in CO_2. The MT properties of the EHP can be investigated at low hydrogen concentrations since the diffusion pathways in the gas phase increase. Furthermore, 1 % CO was added to the gas mix to probe the effect of the binders on catalyst poisoning.

A high hydrogen recovery rate is crucial for achieving high system efficiency. Since H_2 exhibits fast diffusion rates, the operation under low stoichiometries is feasible [54]. At low stoichiometries, the MT becomes the dominant resistance, and local gas depletion might lead to carbon oxidation, irreversibly degrading the CL [55]. A high temperature is essential for the operation of the EHP with gas mixes at low λ, since it improves the diffusion and reduces the Pt poisoning by CO. Fig. 8a presents the PPFSt-Imi-C10 + Triton X-100 EHP at different H_2 recovery rates at 200 °C. As described above, power consumption increases significantly due to MT losses at high H_2 recovery rates. However, the EHP can still be operated at 100 % H_2 recovery rate, even with this challenging gas feed. At 0.2 A cm^{-2} a power efficiency of 95 % was reached, which drops to 78 % at 1.0 A cm^{-2} due to increasing MT losses (see Fig. 8b).

Fig. 8c compares all cells operated at 100 % H_2 recovery. PWN70 and PPFSt-Imi-C10 + Triton X-100 perform similarly well. EIS and the distribution of relaxation times (DRT) in part II undertake a detailed investigation of the underlying resistances contributing to the performance [32]. It was found that the better performance of the tested ionomers compared to PTFE mainly lies in a reduced cathode resistance. The improved PA distribution resulting from the interaction of PA with the PWN70 and PPFSt-Imi-C10 + Triton X-100 binders may increase the TPB, thereby improving the kinetics in both electrodes. Since the different processes taking place in electrochemical systems are often closely linked, the improved proton conduction in the electrodes might also further promote the HER. Furthermore, a slight improvement in the anode kinetics was detected with the PWN70 binder. The ionomer may reduce phosphate anion adsorption on the Pt surface, thereby promoting the hydrogen oxidation reaction (HOR). Also, the excellent film formation over the Pt particles could reduce the CO adsorption on the catalyst, thereby improving the electrochemically active SA.

PTFE, PWN70, and PPFSt-Imi-10 + Triton X-100 showed a similar low MT, resulting in relatively linear PCs (see part II [32]). While the high porosity of the PWN70 CL facilitates the MT, the hydrophilic binder draws more PA in the electrode. The high PA content in the CL worsens the MT, but apparently, both effects seem to balance each other. Furthermore, the phosphonic acid groups of PWN70 influence the PA distribution, possibly supporting the formation of a thin PA film over the CL structure. Subsequently, less PA blocks pores, which severely hampers the MT. The PTFE binder produces a less porous CL, but the hydrophobic material also reduces the PA movement into the CL. This trend continues for the PPFSt-Imi-10 + Triton X-100 CL, which is less porous but more hydrophobic. Despite the significantly lower SA and porosity, PPFSt-imi-C10 + Triton X-100 performs similarly to the PWN70 GDE. The higher hydrophobicity of PPFSt-Imi reduces the PA content in the GDE, thereby improving the MT in the CL. All binders provide a suitable MT due to a combination of their morphological and physical properties, although these are different.

The HOR kinetics are the primary reason for the limited performance of the PPFSt-Imi cells without surfactant (see Part II [32]). The discontinuous binder film produces a low TPB, especially if CO poisons the active Pt area in the gas feed. If the binder distribution is improved by the addition of Triton X-100, the PPFSt-Imi binder performs significantly better. Therefore, the intrinsic properties of these materials are suitable for EHPs, but a sophisticated ink composition is necessary to achieve a well-structured CL. Furthermore, the hydrophobicity of the binder is easily tunable by adjusting the length of the alkyl chain. Therefore, the binder properties can be adjusted to suit different membranes or carbon structures to achieve the optimal PA content in the CL for the specific application.

The dependency of the H_2 quality on the current density is presented in Fig. 9. Each data point represents a single gas sample taken under identical conditions in each of the 5 investigated EHPs, and every sample was measured twice. The indicated error bars display the standard deviation of all 10 measurements. In the investigated current range, the gas purity scales almost linearly with the current. Increasing the current leads to a higher H_2 flow through the membrane, while contaminants diffuse through the membrane independently of the current. The gas

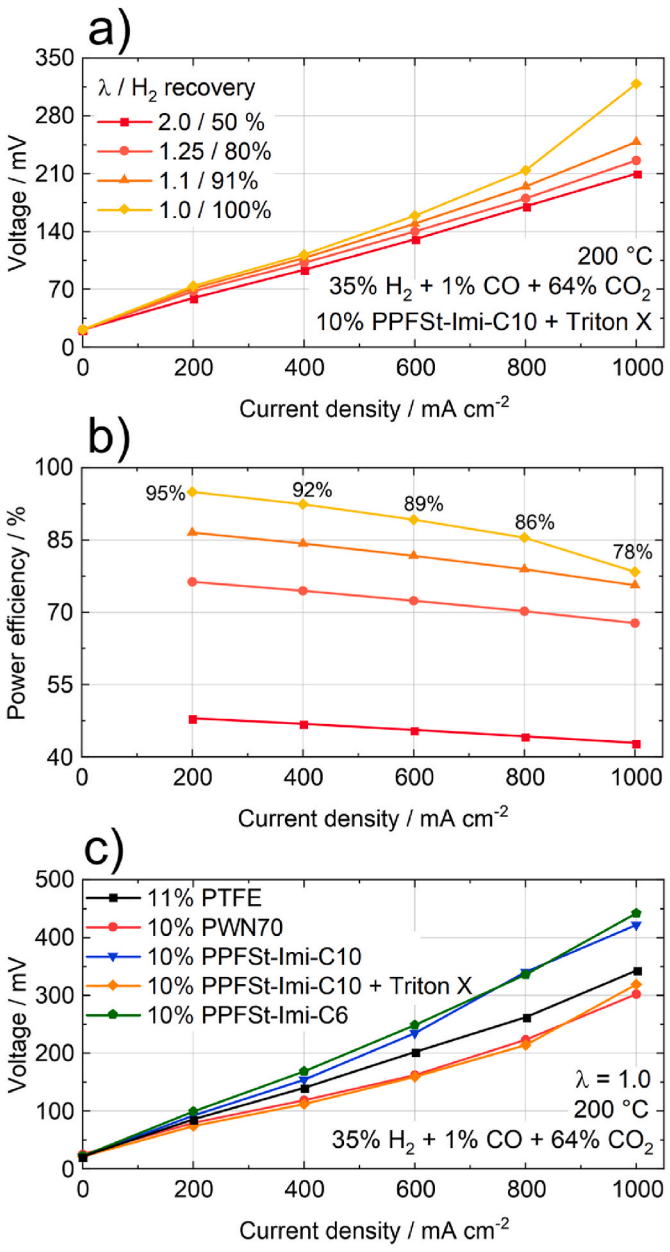

Fig. 8. a) Polarization curves of the EHP with 10 % PPFSt-Imi-C10 binder and Triton X-100 at different H_2 recovery rates from 35 % H_2 + 1 % CO + 64 % CO_2 at 200 °C, and b) the corresponding total efficiency. c) The polarization curves at 100 % H_2 recovery from the same gas mix for all tested EHPs at 200 °C.

quality improves since a constant flow of the contaminants towards the cathode is increasingly "diluted" by a higher H_2 flow at high currents. This trend is observed for both pollutants. Furthermore, the gas purity is lower at 200 °C compared to 180 °C, which might be caused by a faster diffusion rate through the membrane at elevated temperature. However, the error bars overlap at every operation point, so this trend might only be an artifact due to insufficient data. The H_2 recovery rate has no significant impact on the gas quality.

The H_2 purity is 99.98 % at 0.6 A cm^{-2}, which is suitable for most hydrogen applications. However, a 2 ppm CO concentration is too high for Nafion-based fuel cells, so a second EHP could be employed to further purify this gas stream. If another EHP is connected in series, its power consumption would be significantly lower, as no relevant contaminant concentrations are present in the gas stream. Subsequently, the kinetic and MT resistances decrease particularly, and the EHP can

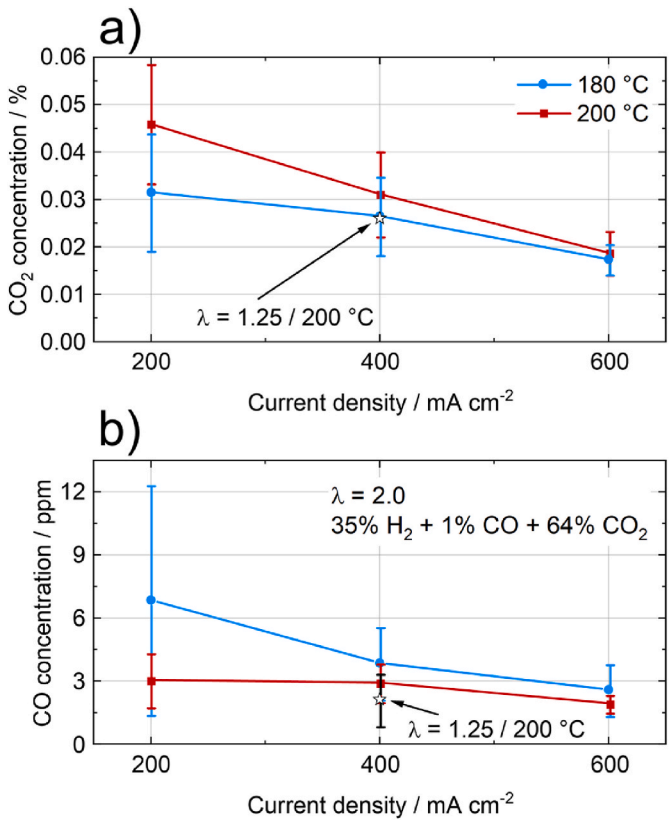

Fig. 9. a) CO_2 and b) CO concentrations of the cathode outlet gas using 35 % H_2 + 1 % CO + 64 % CO_2 with λ = 2.0 at 180 and 200 °C over the current density. The star indicates the respective concentrations at λ = 1.25 and 200 °C measured in the 10 % PWN70 EHP with H14CX653 GDL.

also be operated at a lower temperature, such as 160 °C. Furthermore, less catalyst loading is required, which renders a two-EHP system in series a feasible option if very pure H_2 is required.

To reduce the EHP cost, a lower catalyst loading could be achieved by implementing platinum alloys or other platinum group metals (PGMs). On the anode of PEM fuel cells, PtRu reduces CO poisoning, allowing for a reduction in catalyst loading without compromising performance [56]. It has already been proven in an EHP with Nafion ionomer that Ir retains good performance in a CO_2 atmosphere, while exhibiting similar activity towards the HOR as Pt [57]. Thus, both catalysts are also promising as future anode catalysts in EHPs.

A durability test with an EHP containing PWN70 binder and a H23C2 MPL is presented in Fig. 10. The PC is nearly identical to the previously investigated cell with 10 % PWN70 on an H14CX653 GDL, so the long-term operation is likely transferrable (see Fig. 10a). To our knowledge, we demonstrate for the first time that an EHP can be operated up to 2.0 A cm^2 at λ = 1.0 with a gas feed containing CO and CO2, highlighting the excellent performance of the fabricated GDEs. In the investigated range, no limiting current was observed, which indicates excellent diffusion properties of the CL. Since the fabricated ionomers can be operated at only 0.7 % RH, flooding is consistently prevented. EHPs with Nafion ionomers showed a limiting current around ~2.0 A cm^{-2} with (almost) pure H_2 gas feed [8,58], and only ~0.3 A cm^{-2} with 1000 ppm CO and 20 % CO_2 in H_2 [5], which demonstrates the superior performance of the PA-doped PWN70 ionomer. Another study showed high voltages at only 0.2 A cm-2 with Nafion as the ionomer, using a gas feed of 40 % H2 and 60 % CO2 [59]. However, it should be noted that the platinum loading in the catalyst layers was lower than in the present work.

The EHP exhibited a relatively stable voltage of 1.6 A cm^{-2} over 169 h, although the cell voltage increased from 650 to 720 mV within the first 24 h (see Fig. 10b). Due to the low stoichiometry and CO poisoning,

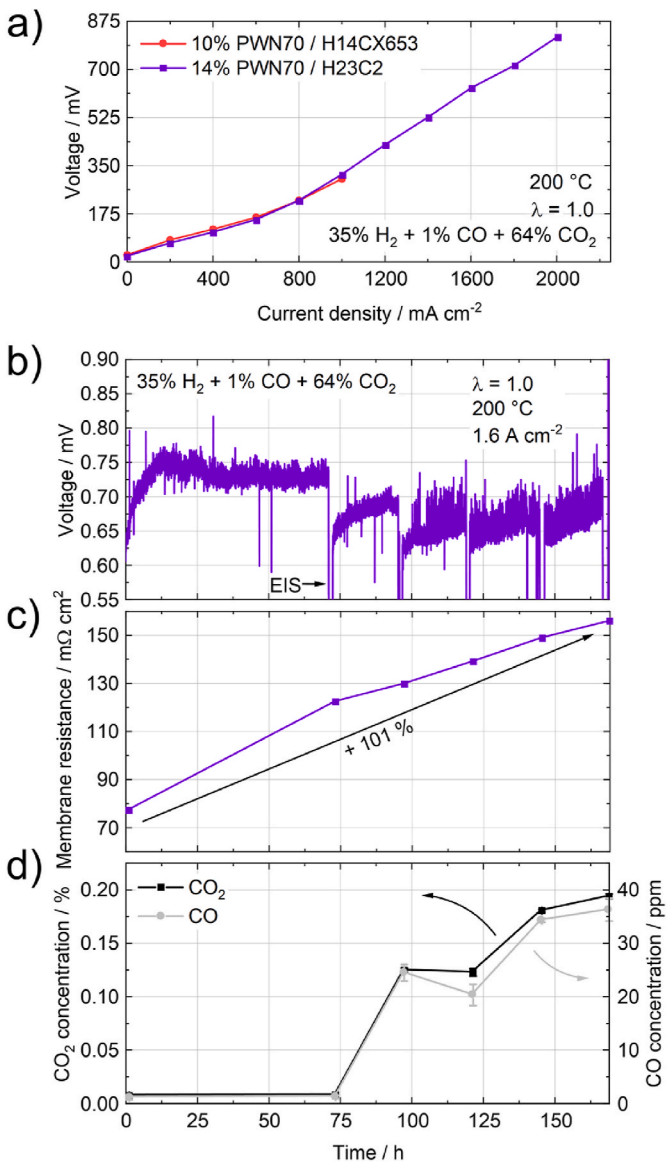

Fig. 10. a) Polarization curve of the EHP for long-term testing with 14 % PWN70 binder and a H23C2 GDL at λ = 1.0 with 35 % H_2 + 1 % CO + 64 % CO_2 gas feed at 0.7 % RH and 200 °C compared to the EHP with 10 % PWN70 and a H14CX653 GDL previously shown in Fig. 8c b) EHP voltage, c) membrane resistance, and d) H_2 contaminations during a stability test at a constant current of 1.6 A cm^{-2} under the same conditions as a).

the cell voltage fluctuates approximately 50 mV, but this does not seem to degrade the catalyst. The carbon corrosion is significantly slower in a PA-doped electrode operated at 160 °C compared to a PFSA ionomer at 23 °C [60]. Furthermore, the onset potential for carbon corrosion was determined to be 0.9 V in the electrode with PA. Since the EHP was operated below this voltage, pronounced carbon corrosion was avoided.

The PBI membrane degrades during operation at 200 °C, resulting in an increase in membrane resistance. Fig. 10c). Furthermore, the membrane disintegration is also evident in the decreasing gas quality over time (see Fig. 10d). Tiny defects in the membrane film allow contaminants to move from the anode to the cathode, increasing the CO and CO_2 content in the purified hydrogen. Additionally, phosphoric acid likely evaporates from PBI at high temperatures, which also contributes to an increase in the membrane resistance [61]. Replacing the PBI with an ion-pair membrane might enhance the cell's lifetime due to its higher thermal stability and improved acid retention.

Until 75 h, a H_2 quality of 99.99 % was achieved, surpassing results from the literature with similar gas feeds [3,10–12,16]. At the end of the durability test, the H_2 purity drops to 99.80 %, which is insufficient for fuel cell vehicles [62,63]. However, this value is still above the quality measured in an ion-pair-based EHP after 100 h operation at 0.25 A cm^{-2}, where a drop from 99.65 % (start) to 99.47 % was measured with a gas feed containing 25 % H_2 [12].

4. Conclusions

GDEs were fabricated with three poly(pentafluorstyrene) (PPFSt) based ionomers and PTFE as binders. The ionomers were synthesized by attaching imidazole to a PPFSt chain, followed by alkylation of the imidazole ring with hexyl (C6) and decyl (C10) chains. The inks for all ionomers were prepared with a high IPA content since dynamic light scattering revealed smaller binder particles in inks with a high IPA share. SEM and EDX indicated an excellent ionomer distribution in the CLs. While PTFE forms agglomerations with a diameter of few µm in the CL, all ionomers were well dispersed, and no agglomerations were identified. The highest CL porosity was achieved with PWN70, which is one reason for its excellent performance. PPFSt-Imi-C6 and -C10 binders produced less porous electrodes; however, adding the surfactant Triton X-100 increased the porosity. The PPFSt-Imi CLs also showed lower water sorption than the PTFE CL, suggesting high hydrophobicity. This finding highlights the importance of the distribution of the ionomers in the electrode, which is more relevant for the hydrophobicity of the electrode than the properties of the individual binder material in this case.

Full-cell EHPs were assembled with the fabricated GDEs and a PA-doped commercial PBI membrane. EHPs with PWN70 ionomer exhibited superior performance with pure H_2 gas feed at 160 and 180 °C, indicating high proton conductivity in the MEA. While the PPFSt-Imi ionomers showed relatively poor performance at 160 °C, the temperature increase to 180 °C reduced the power consumption of the corresponding EHPs significantly. Adding Triton X-100 further improved the performance, as it formed a more homogeneous CL morphology.

At 200 °C cell temperature, all EHPs isolated H_2 from a gas mix containing 35 % H_2 + 1 % CO + 64 % CO_2 at 100 % H_2 recovery. The cells with the PWN70 and PPFSt-Imi-C10 + Triton X-100 GDEs showed similar performance, and both outperformed the standard PTFE binder. At 0.2 A cm^{-2}, a power efficiency of 95 % was reached.

A GDE containing PWN70 ionomer demonstrated stable performance in a durability test over 169 h at 1.6 A cm^{-2} and 100 % H_2 recovery. A high H_2 purity was achieved between 99.95 % (0.2 A cm^{-2}) and 99.99 % (1.6 A cm^{-2}) with below 3 ppm CO.

CRediT authorship contribution statement

M. Braig: Writing – original draft, Visualization, Methodology, Investigation, Formal analysis, Data curation. **H. Cho:** Writing – review & editing, Investigation, Formal analysis, Data curation. **C. Marchfelder:** Writing – review & editing, Investigation, Formal analysis, Data curation. **V. Atanasov:** Writing – review & editing, Supervision, Project administration, Funding acquisition, Formal analysis. **R. Zeis:** Writing – review & editing, Supervision, Project administration, Methodology, Investigation, Funding acquisition, Conceptualization.

Declaration of competing interest

The authors declare that they have no known competing financial interests or personal relationships that could have appeared to influence the work reported in this paper.

Acknowledgements

The authors thank the ZSW (Zentrum für Sonnenenergie und Wasserstoff-Forschung) Ulm for providing the hydrogen test stations

infrastructure. This work contributes to the research performed at CELEST (Center for Electrochemical Energy Storage Ulm-Karlsruhe).

Appendix A. Supplementary data

Supplementary data to this article can be found online at https://doi.org/10.1016/j.ijhydene.2025.151219.

References

[1] Ströbel R, Oszcipok M, Fasil M, Rohland B, Jörissen L, Garche J. The compression of hydrogen in an electrochemical cell based on a PE fuel cell design. J Power Sources 2002;105:208–15. https://doi.org/10.1016/S0378-7753(01)00941-7.

[2] Yang R, Kweon H, Kim K. Preliminary study for the commercialization of a electrochemical hydrogen compressor. Energies 2023;16. https://doi.org/10.3390/en16073128.

[3] Thomassen M, Sheridan E, Kvello J. Electrochemical hydrogen separation and compression using polybenzimidazole (PBI) fuel cell technology. J Nat Gas Sci Eng 2010;2:229–34. https://doi.org/10.1016/j.jngse.2010.10.002.

[4] Lepage T, Kammoun M, Schmetz Q, Richel A. Biomass-to-hydrogen: a review of main routes production, processes evaluation and techno-economical assessment. Biomass Bioenergy 2021;144:105920. https://doi.org/10.1016/j.biombioe.2020.105920.

[5] Gardner CL, Ternan M. Electrochemical separation of hydrogen from reformate using PEM fuel cell technology. J Power Sources 2007;171:835–41. https://doi.org/10.1016/j.jpowsour.2007.06.020.

[6] Abdulla A, Laney K, Padilla M, Sundaresan S, Benziger J. Efficiency of hydrogen recovery from reformate with a polymer electrolyte hydrogen pump. AIChE J 2011;57:1767–79. https://doi.org/10.1002/aic.12406.

[7] Trégaro M, Rhandi M, Druart F, Deseure J, Chatenet M. Electrochemical hydrogen compression and purification versus competing technologies: part II. Challenges in electrocatalysis. Chin J Catal 2020;41:770–82. https://doi.org/10.1016/S1872-2067(19)63438-8.

[8] Jackson C, Raymakers LFJM, Mulder MJJ, Kucernak ARJ. Poison mitigation strategies for the use of impure hydrogen in electrochemical hydrogen pumps and fuel cells. J Power Sources 2020;472:228476. https://doi.org/10.1016/j.jpowsour.2020.228476.

[9] Wu X, He G, Yu L, Li X. Electrochemical hydrogen pump with speek/CrPSSA semi-interpenetrating polymer network proton exchange membrane for H2/CO2 separation. ACS Sustainable Chem Eng 2014;2:75–9. https://doi.org/10.1021/sc400329s.

[10] Huang F, Pingitore AT, Benicewicz BC. Electrochemical hydrogen separation from reformate using high-temperature polybenzimidazole (PBI) membranes: the role of chemistry. ACS Sustainable Chem Eng 2020;8:6234–42. https://doi.org/10.1021/acssuschemeng.9b07037.

[11] Huang F, Pingitore AT, Benicewicz BC. High polymer content m/p-Polybenzimidazole copolymer membranes for electrochemical hydrogen separation under differential pressures. J Electrochem Soc 2020;167:063504. https://doi.org/10.1149/1945-7111/ab81a0.

[12] Venugopalan G, Bhattacharya D, Andrews E, Briceno-Mena L, Romagnoli J, Flake J, et al. Electrochemical pumping for challenging hydrogen separations. ACS Energy Lett 2022;7:1322–9. https://doi.org/10.1021/acsenergylett.1c02853.

[13] Rhandi M, Trégaro M, Druart F, Deseure J, Chatenet M. Electrochemical hydrogen compression and purification versus competing technologies: part I. Pros and cons. Chin J Catal 2020;41:756–69. https://doi.org/10.1016/S1872-2067(19)63404-2.

[14] Bernardo G, Araújo T, da Silva Lopes T, Sousa J, Mendes A. Recent advances in membrane technologies for hydrogen purification. Int J Hydrogen Energy 2020;45:7313–38. https://doi.org/10.1016/j.ijhydene.2019.06.162.

[15] Braig M, Zeis R. Distribution of relaxation times analysis of electrochemical hydrogen pump impedance spectra. J Power Sources 2023;576:233203. https://doi.org/10.1016/j.jpowsour.2023.233203.

[16] Perry KA, Eisman GA, Benicewicz BC. Electrochemical hydrogen pumping using a high-temperature polybenzimidazole (PBI) membrane. J Power Sources 2008;177:478–84. https://doi.org/10.1016/j.jpowsour.2007.11.059.

[17] Petek TJ, Wainright JS, Savinell RF. High temperature electrochemical hydrogen pump cell using a PBI membrane at high current densities. ECS Meet Abstr 2012;MA2012–02. https://doi.org/10.1149/ma2012-02/13/1702. 1702–1702.

[18] Mack F, Morawietz T, Hiesgen R, Kramer D, Gogel V, Zeis R. Influence of the polytetrafluoroethylene content on the performance of high-temperature polymer electrolyte membrane fuel cell electrodes. Int J Hydrogen Energy 2016;41:7475–83. https://doi.org/10.1016/j.ijhydene.2016.02.156.

[19] Adhikari S, Leonard DP, Lim KH, Park EJ, Fujimoto C, Morales-Collazo O, et al. Hydrophobic quaternized poly(fluorene) ionomers for emerging fuel cells. ACS Appl Energy Mater 2022;5:2663–8. https://doi.org/10.1021/acsaem.2c00119.

[20] Atanasov V, Lee AS, Park EJ, Maurya S, Baca ED, Fujimoto C, et al. Synergistically integrated phosphonated poly(pentafluorostyrene) for fuel cells. Nat Mater 2021;20:370–7. https://doi.org/10.1038/s41563-020-00841-z.

[21] Kim YS. Hydrocarbon ionomeric binders for fuel cells and electrolyzers. Adv Sci 2023:2303914. https://doi.org/10.1002/advs.202303914. 1–32.

[22] Atanasov V, Oleynikov A, Xia J, Lyonnard S, Kerres J. Phosphonic acid functionalized poly(pentafluorostyrene) as polyelectrolyte membrane for fuel cell application. J Power Sources 2017;343:364–72. https://doi.org/10.1016/j.jpowsour.2017.01.085.

[23] Lim K, Lee A, Atanasov V. Protonated phosphonic acid electrodes for high power heavy-duty vehicle fuel cells. 2008.

[24] Park JO, Kwon K, Cho MD, Hong S-G, Kim TY, Yoo DY. Role of binders in high temperature PEMFC electrode. J Electrochem Soc 2011;158:B675–81. https://doi.org/10.1149/1.3573773.

[25] Tang H, Geng K, Aili D, Ju Q, Pan J, Chao G, et al. Low Pt loading for high-performance fuel cell electrodes enabled by hydrogen-bonding microporous polymer binders. Nat Commun 2022;13. https://doi.org/10.1038/s41467-022-34489-x.

[26] Melchior JP, Majer G, Kreuer KD. Why do proton conducting polybenzimidazole phosphoric acid membranes perform well in high-temperature PEM fuel cells? Phys Chem Chem Phys 2017;19:601–12. https://doi.org/10.1039/c6cp05331a.

[27] Cho H, Seiler J, Atanasova P, Atanasov V. Ion-pair membrane based on imidazolium-functionalized poly(pentafluorostyrene) for high-temperature proton exchange membrane fuel cell application. https://doi.org/10.1021/acsaem.3c02854; 2024.

[28] Atanasov V, Kerres J. Highly phosphonated polypentafluorostyrene. Macromolecules 2011;44:6416–23. https://doi.org/10.1021/ma2011574.

[29] Shukla S, Bhattacharjee S, Weber AZ, Secanell M. Experimental and theoretical analysis of ink dispersion stability for polymer electrolyte fuel cell applications. J Electrochem Soc 2017;164:F600–9. https://doi.org/10.1149/2.0961706jes.

[30] Lee WJ, Lee JS, Park HY, Park HS, Lee SY, Song KH, et al. Improvement of fuel cell performances through the enhanced dispersion of the PTFE binder in electrodes for use in high temperature polymer electrolyte membrane fuel cells. Int J Hydrogen Energy 2020;45:32825–33. https://doi.org/10.1016/j.ijhydene.2020.03.095.

[31] Arslan F, Dirsch J, Wagner M, Freiberg ATS, Komma M, Kerres J, et al. The influence of intrinsically proton conductive electrode binder materials on HT-PEMFC performance. J Power Sources 2023;553. https://doi.org/10.1016/j.jpowsour.2022.232297.

[32] Braig M, Cho H, Marchfelder C, Atanasov V, Zeis R. Poly(pentafluorstyrene) based ionomers for electrochemical hydrogen pumps with 100% H2 recovery II – probing the electrode processes with EIS and DRT. Int J Hydrogen Energy 2024.

[33] Pingitore AT, Huang F, Qian G, Benicewicz BC. Durable high polymer content m/p-Polybenzimidazole membranes for extended lifetime electrochemical devices. ACS Appl Energy Mater 2019;2:1720–6. https://doi.org/10.1021/acsaem.8b01820.

[34] Liu H, Ney L, Zamel N, Li X. Effect of catalyst ink and formation process on the multiscale structure of catalyst layers in PEM fuel cells. Appl Sci 2022;12. https://doi.org/10.3390/app12083776.

[35] Jung J, Lim KH, Maurya S, Manriquez LD, Atanasov V, Ahn CH, et al. Dispersing agents impact performance of protonated phosphonic acid high-temperature polymer electrolyte membrane fuel cells. ACS Energy Lett 2022:1642–7. https://doi.org/10.1021/acsenergylett.2c00359.

[36] Song CH, Park JS. Effect of dispersion solvents in catalyst inks on the performance and durability of catalyst layers in proton exchange membrane fuel cells. Energies 2019;12. https://doi.org/10.3390/en12030549.

[37] Doo G, Lee JH, Yuk S, Choi S, Lee DH, Lee DW, et al. Tuning the ionomer distribution in the fuel cell catalyst layer with scaling the ionomer aggregate size in dispersion. ACS Appl Mater Interfaces 2018;10:17835–41. https://doi.org/10.1021/acsami.8b01751.

[38] Anderson W, Kozak D, Coleman VA, Jämting ÅK, Trau M. A comparative study of submicron particle sizing platforms: Accuracy, precision and resolution analysis of polydisperse particle size distributions. J Colloid Interface Sci 2013;405:322–30. https://doi.org/10.1016/j.jcis.2013.02.030.

[39] Mack F, Klages M, Scholta J, Jörissen L, Morawietz T, Hiesgen R, et al. Morphology studies on high-temperature polymer electrolyte membrane fuel cell electrodes. J Power Sources 2014;255:431–8. https://doi.org/10.1016/j.jpowsour.2014.01.032.

[40] Huang DC, Yu PJ, Liu FJ, Huang SL, Hsueh KL, Chen YC, et al. Effect of dispersion solvent in catalyst ink on proton exchange membrane fuel cell performance. Int J Electrochem Sci 2011;6:2551–65. https://doi.org/10.1016/s1452-3981(23)18202-2.

[41] Lin HL, Yu TL, Shen KS, Huang LN. Effect of Triton-X on the preparation of Nafion/PTFE composite membranes. J Membr Sci 2004;237:1–7. https://doi.org/10.1016/j.memsci.2004.01.021.

[42] Freudenberg Performance Materials SE & Co. KG. Freudenberg gas diffusion layer - fuel cell technical data. 2021.

[43] Braig M, Deissler NH, Lüdeking I, Regnet F, Bevilacqua N, Zeis R. FIB-SEM and ToF-SIMS analysis of high-temperature PEM fuel cell electrodes. Adv Mater Interfac 2023;10. https://doi.org/10.1002/admi.202202430.

[44] Mack F, Morawietz T, Hiesgen R, Kramer D, Zeis R. PTFE distribution in high-temperature PEM electrodes and its effect on the cell performance. ECS Trans 2013;58:881–8. https://doi.org/10.1149/05801.0881ecst.

[45] Liu S, Wippermann K, Lehnert W. Mechanism of action of polytetrafluoroethylene binder on the performance and durability of high-temperature polymer electrolyte fuel cells. Int J Hydrogen Energy 2021;46:14687–98. https://doi.org/10.1016/j.ijhydene.2021.01.192.

[46] Li D, Chung HT, Maurya S, Matanovic I, Kim YS. Impact of ionomer adsorption on alkaline hydrogen oxidation activity and fuel cell performance. Curr Opin Electrochem 2018;12:189–95. https://doi.org/10.1016/j.coelec.2018.11.012.

[47] Thommes M, Kaneko K, Neimark AV, Olivier JP, Rodriguez-Reinoso F, Rouquerol J, et al. Physisorption of gases, with special reference to the evaluation of surface area and pore size distribution (IUPAC technical report). Pure Appl Chem 2015;87:1051–69. https://doi.org/10.1515/pac-2014-1117.

[48] Landers J, Gor GY, Neimark AV. Density functional theory methods for characterization of porous materials. Colloids Surfaces A Physicochem Eng Asp 2013;437:3–32. https://doi.org/10.1016/j.colsurfa.2013.01.007.

[49] Soboleva T, Malek K, Xie Z, Navessin T, Holdcroft S. PEMFC catalyst layers: the role of micropores and mesopores on water sorption and fuel cell activity. ACS Appl Mater Interfaces 2011;3:1827–37. https://doi.org/10.1021/am200590w.
[50] Zhang R, Yang B, Shao Z, Yang D, Ming P, Li B, et al. Graph theory model and mechanism analysis of carbon fiber paper conductivity in fuel cell based on physical structure. J Power Sources 2021;491:229546. https://doi.org/10.1016/j.jpowsour.2021.229546.
[51] Korte C. Phosphoric acid, an electrolyte for fuel cells - temperature and composition dependence of vapor pressure and proton conductivity. Fuel Cell Sci Eng Mater Process Syst Technol 2012;1:335–59. https://doi.org/10.1002/9783527650248.ch12.
[52] Melchior JP, Kreuer KD, Maier J. Proton conduction mechanisms in the phosphoric acid-water system (H4P2O7-H3PO4·2H2O): a 1H, 31P and 17O PFG-NMR and conductivity study. Phys Chem Chem Phys 2017;19:587–600. https://doi.org/10.1039/c6cp04855b.
[53] Lee AS, Choe YK, Matanovic I, Kim YS. The energetics of phosphoric acid interactions reveals a new acid loss mechanism. J Mater Chem A 2019;7:9867–76. https://doi.org/10.1039/c9ta01756a.
[54] Halter J, Thomas S, Kær SK, Schmidt TJ, Büchi FN. The influence of phosphoric acid migration on the performance of high temperature polymer electrolyte fuel cells. J Power Sources 2018;399:151–6. https://doi.org/10.1016/j.jpowsour.2018.07.090.
[55] Yezerska K, Liu F, Dushina A, Sergeev O, Wagner P, Dyck A, et al. Analysis of the regeneration behavior of high temperature polymer electrolyte membrane fuel cells after hydrogen starvation. J Power Sources 2020;449:227562. https://doi.org/10.1016/j.jpowsour.2019.227562.
[56] Antolini E, Giorgi L, Cardellini F, Passalacqua E. Physical and morphological characteristics and electrochemical behaviour in PEM fuel cells of PtRu/C catalysts. J Solid State Electrochem 2001;5:131–40. https://doi.org/10.1007/s100080000116.
[57] Kim SJ, Park HY, Ahn SH, Lee B seok, Kim HJ, Cho EA, et al. Highly active and CO2 tolerant Ir nanocatalysts for H2/CO2 separation in electrochemical hydrogen pumps. Appl Catal B Environ 2014;158–159:348–54. https://doi.org/10.1016/j.apcatb.2014.04.016.
[58] Zeng Y, Li J, Li M, Yang S, Wang J, Hou J, et al. Electrochemical hydrogen pump based on proton exchange membrane for rapid separation of hydrogen and helium. Int J Hydrogen Energy 2024;63:418–23. https://doi.org/10.1016/j.ijhydene.2024.03.128.
[59] Yang W, Sun X, Li J, Tang C, Xie P, Shao W, et al. The effect of concentration polarization and chemical interactions on electrochemical hydrogen pump. Int J Hydrogen Energy 2024;52:485–90. https://doi.org/10.1016/j.ijhydene.2023.11.034.
[60] Cremers C, Jurzinsky T, Meier J, Schade A, Branghofer M, Pinkwart K, et al. DEMS and online mass spectrometry studies of the carbon support corrosion under various polymer electrolyte membrane fuel cell operating conditions. J Electrochem Soc 2018;165:F3307–15. https://doi.org/10.1149/2.0331806jes.
[61] Kannan A, Li Q, Cleemann LN, Jensen JO. Acid distribution and durability of HT-PEM fuel cells with different electrode supports. Fuel Cells 2018;18:103–12. https://doi.org/10.1002/fuce.201700181.
[62] Aarhaug TA, Kjos O, Bacquart T, Valter V, Optenhostert T. Assessment of hydrogen quality dispensed for hydrogen refuelling stations in Europe. Int J Hydrogen Energy 2021;46:29501–11. https://doi.org/10.1016/j.ijhydene.2020.11.163.
[63] International Organization for Standardization. Hydrogen fuel quality — product specification. 2019.